

Microseismic focal mechanisms: A tutorial

David W. Eaton

ABSTRACT

Techniques for characterizing seismic sources, borrowed from earthquake seismology, can provide useful information for microseismic studies. Various magnitude scales are used in earthquake seismology, the oldest of which (Richter magnitude) is specific to California earthquakes. All such scales are logarithmic and yield an estimated 30-fold increase in radiated seismic energy per unit magnitude increment. Simple models of fault displacement yield acceleration and displacement spectra from which seismic moments and corner frequencies can be determined. The corner frequency, in turn, may be used to estimate stress drop and source radius. The seismic moment tensor provides a general description of a source in terms of force couples, of which several types are of particular interest for microseismic studies. Double-couple sources describe slip on existing fracture surfaces, whereas tensile compensated linear vector dipole (CLVD) mechanisms describe a plausible mechanism for generation of new fractures within a competent rock mass. The role of stress transfer in earthquake occurrence has recently been recognized. Coulomb stress change provides a simple predictive model for discriminating between regions that move close to (or farther from) failure in the aftermath of an earthquake. Such models may have application to far-field induced seismicity associated with hydraulic fracturing.

INTRODUCTION

Microseismic methods have emerged as an important tool for monitoring fluid processes at the reservoir scale. Microseismic activity in a subsurface reservoir may result from brittle deformation of reservoir rocks due to fluid injection. The ability to pinpoint the locations of microseismic events provides a basis for tracking the movement of fluids and investigating the state of stress in the reservoir. Applications of microseismic monitoring have included mapping microseismic activity induced during a program of cyclic steam stimulation (McGillivray, 2005) or CO₂ sequestration (White et al. 2004), and monitoring and characterization of hydraulic fracturing (Nolen-Hoeksema and Ruff, 2001; Sasaki and Kaieda, 2002; Rutledge and Phillips, 2003).

In many cases, the primary objectives of microseismic monitoring are to detect and precisely locate all seismic activity above a given magnitude threshold. This is typically accomplished using methods that are drawn from earthquake seismology, where relevant techniques are well documented in the literature. Beyond such first-order questions of the location and distribution of seismic activity, given sufficiently good data quality microseismic events can be characterized more completely using other earthquake-related techniques. Such characterization may include spectral analysis for determination of rupture dimensions and stress drop, moment-tensor inversion and changes in the Coulomb stress field.

The purpose of this tutorial is to provide a concise review of selected methods for characterizing microseismic sources. Although the background theory is developed from

the perspective of earthquake seismology, the techniques described are inherently scalable and broadly applicable to microseismic monitoring at the reservoir scale.

DESCRIPTION OF SEISMIC SOURCES

Magnitude

The task of measuring the *size* of an earthquake or other seismic event can be compared to finding the dimensions of an abstract sculpture, since the result depends very strongly on how one chooses to make the measurement. Nevertheless, since the introduction of a local California magnitude scale in the 1930's by Charles Richter, the concept of earthquake magnitude based on a logarithmic representation of measured ground motion has become entrenched. In quantitative evaluation of earthquake magnitude, terminology is important since various scales are in common use - although the distinction between the different types of earthquake magnitude is often overlooked.

The general formula for earthquake magnitude may be written as

$$M = \log_{10}(A/T^n) + Q(h, \Delta), \quad (1)$$

where A is peak ground displacement, typically measured in μm for a specific seismic wave type (e.g., Rayleigh), T is dominant period in seconds, $n = 0$ or 1 and Q is an empirical function of source depth (h) and distance (Δ). In the case of Richter magnitude, this formula takes the specific form (Bullen and Bolt, 1985)

$$M_L = \log_{10}(A) + 2.56 \log_{10} \Delta - 1.67, \quad (2)$$

where Δ is distance in km and A is amplitude recorded on a Wood-Anderson seismograph, an historical instrument with a narrow-band response ~ 0.8 s. Although routinely cited for many other applications, this scale is strictly valid for California earthquakes in the distance range $10 < \Delta < 600$ km. Furthermore, since Wood-Anderson seismographs are no longer used, it is necessary to filter the recorded signal to simulate the instrument response.

An alternative local magnitude scale proposed by Nuttli (1973) is in widespread use in eastern North America. The Nuttli magnitude is given by

$$m_N = \log_{10}(A/T) + 0.90 \log_{10}(\Delta) + 3.75, \quad (3)$$

where A is measured using the S wave arrival and Δ is angular distance in degrees (i.e., the angle subtended at Earth's centre between the epicenter and the station). Large earthquakes are often reported in global seismic catalogs using other scales, such as body-wave magnitude (m_b) and surface-wave magnitude (M_s). It is customary to use lower case m to designate a magnitude derived from body-wave amplitude, and upper case M to designate a magnitude derived mainly from surface waves.

The most definitive scalar measure of earthquake size is the seismic moment, given by

$$M_0 = \mu DA, \quad (4)$$

where μ is the shear modulus, D is average co-seismic displacement and A is the fault area. The scalar seismic moment may be converted to so-called moment magnitude using the following formula:

$$M_w = \frac{2}{3} \log_{10}(M_0) - 10.7 \quad (5)$$

This is the preferred reference magnitude scale in earthquake seismology, since it corresponds closely with other scales (e.g., M_s) for most earthquakes but, unlike other magnitude scales, it does not saturate for very large events such as the 2004 Sumatra-Andaman earthquake ($M_w = 9.2$). Since the parameters required to determine the seismic moment (eq. 4) are often difficult or impossible to obtain (especially in the case of reservoir-scale microseismicity), various empirical relations exist between other magnitude scales and M_w .

The total radiated energy from an earthquake can be estimated using (Shearer, 1999)

$$\log_{10} E = 4.8 + 1.5 M_w, \quad (6)$$

where E is in Joules. This equation tells us that each unit increment in magnitude corresponds to a factor of 30 increase in energy release. Thus, the ratio of energy released by the 2004 Sumatra-Andaman earthquake relative to a $M = -2$ microseismic event is about 6×10^{16} .

Source spectrum and stress drop

A simple model for displacement on a fault during an earthquake is given by

$$d(t) = D \left[1 - (1 + t/\tau) e^{-t/\tau} \right], \quad (7)$$

where D is the net displacement (*cf.* eq. 4) and τ is called the rise-time parameter. Figure 1 shows a graph of such a displacement history. The far-field acceleration spectrum of elastic waves radiated from such a source is (Beresnev, 2001)

$$\tilde{a}(\omega) = \frac{M_0 \omega^2}{1 + \left(\frac{\omega}{\omega_c} \right)^2}, \quad (8)$$

where \sim denotes the Fourier transform, $\omega = 2\pi f$ and $\omega_c \equiv 1/\tau$ is called the corner frequency. The corresponding displacement spectrum is given by

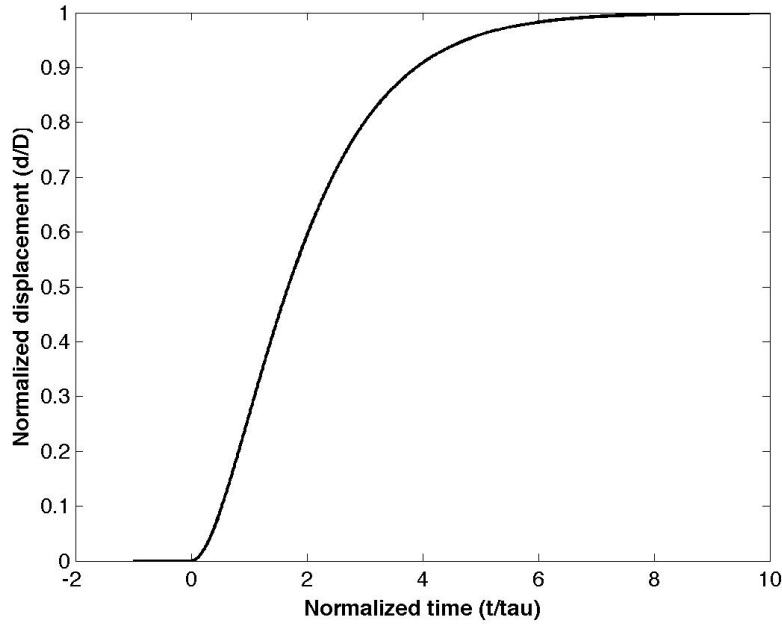


FIG. 1. Simple model for displacement on a fault as described by equation 7.

$$\tilde{d}(\omega) = \frac{M_0}{1 + \left(\frac{\omega}{\omega_c}\right)^2}. \quad (9)$$

The acceleration and displacement spectra are graphed in Figure 2. We see that

$$\lim_{\omega \rightarrow \infty} \tilde{a} = M_0 \omega_c \quad (10)$$

and

$$\lim_{\omega \rightarrow 0} \tilde{d} = M_0. \quad (11)$$

This tells us that the low-frequency limit of the displacement spectrum provides an estimate of the seismic moment. Furthermore, the ratio of the limits in eq. 10 and 11 can be used to estimate the corner frequency, ω_c , which can then be used to estimate the radius of a circular fault (Brune 1970, 1971)

$$R \approx 2.34 \frac{V_s}{\omega_c}, \quad (12)$$

where V_s is the shear-wave velocity of the medium. This provides a crude estimate of the characteristic rupture size, although caution is required in the interpretation of this parameter (Beresnev, 2001). Similarly, we can use the corner frequency to provide a

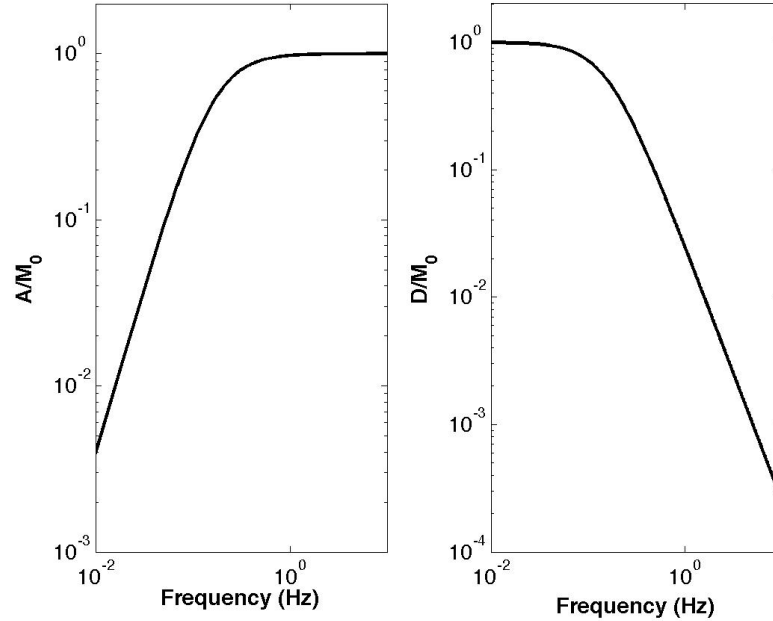


FIG. 2. Far-field acceleration (left) and displacement (right) spectra for the faulting model described by equation 7. Asymptotic limits can be used to determine seismic moment and corner frequency (see text).

crude estimate of the stress drop ($\Delta\sigma$, the average difference between stress on the fault before the earthquake and after the earthquake) using

$$\omega_c \approx 2.34 \times 2V_s \left(\frac{\Delta\sigma}{M_0} \right)^{1/3}. \quad (13)$$

The spectral-derived parameters (R , $\Delta\sigma$) may be useful in passive seismic studies at the reservoir scale for investigating characteristics of microseismicity that are of interest for engineering purposes.

Moment tensors

Besides the spectral analysis described above, another way in which the treatment of seismic sources in earthquake seismology differs from exploration seismology is in the representation of body forces at the source. In earthquake seismology, a general representation of a point source is given by the seismic moment tensor,

$$\mathbf{M} = M_0 \begin{bmatrix} M_{11} & M_{12} & M_{13} \\ M_{21} & M_{22} & M_{23} \\ M_{31} & M_{32} & M_{33} \end{bmatrix}, \quad (14)$$

where each element M_{ij} represents a force couple composed of opposing unit forces pointing in the i -direction, separated by an infinitesimal distance in the j -direction (Figure 3). The moment-tensor formula gives a very flexible representation of seismic waves radiated from a point dislocation. From the perspective of far-field radiated seismic waves, this is a good representation for microseismic sources.

Conservation of angular momentum imposes the condition that \mathbf{M} is symmetric, reducing the number of independent moment-tensor elements to 6 in any co-ordinate system. In general, an arbitrary moment tensor can be diagonalized by eigenvector decomposition. The three eigenvectors define a co-ordinate system that is aligned with the principal stress axes (e.g., Lay and Wallace, 1995).

A particularly simple moment tensor is the double couple. For example,

$$\mathbf{M} = M_0 \begin{bmatrix} 0 & 1/\sqrt{2} & 0 \\ -1/\sqrt{2} & 0 & 0 \\ 0 & 0 & 0 \end{bmatrix}, \quad (15)$$

represents a double-couple mechanism wherein force couples are oriented parallel to the x - and y -axes. Although most earthquakes can be well represented by double-couple mechanisms, other mechanisms are sometimes used. For example, the identity matrix corresponds to an isotropic volumetric expansion (explosion) and the compensated linear vector dipole (CLVD) has a double-strength force couple in the direction of one eigenvector and unit-strength force couples in the directions of the other two (Lay and Wallace, 1995). The latter has been used to represent tensile events that occur in hydraulic fracturing due to nucleation and propagation of the fracture into a competent rockmass (Nolen-Hoeksema and Ruff, 2001).

To see how the moment tensor is used in the calculation of seismic waveforms, consider the momentum equation for an elastic continuum,

$$\rho \ddot{u}_i = \tau_{ij,j} + f_i, \quad (15)$$

where ρ is density, u_i is the i th component of displacement, τ is stress and \mathbf{f} denotes body force. In addition, subscripted commas are used to denote spatial differentiation and Einstein's summation convention for repeated indices has been used. A solution to this equation may be conveniently expressed in terms of a Green's function, $\mathbf{G}(\mathbf{x}, t, \mathbf{x}_0, t_0)$,

$$u_i(\mathbf{x}, t) = G_{ij} f_j(\mathbf{x}_0, t_0), \quad (16)$$

which represents the displacement at \mathbf{x} due to a unit force applied at position \mathbf{x}_0 and time t_0 . In practice, obtaining a Green's function for a complex medium requires either numerical solution to (15) or the use of empirical techniques (Velasco et al., 1994). Given the required Green's function, the displacement may be expressed using the moment tensor source representation as (Shearer, 1999).

$$u_i(\mathbf{x}, t) = \frac{\partial G_{ij}}{\partial x_k} M_{jk}(\mathbf{x}_0, t_0). \quad (17)$$

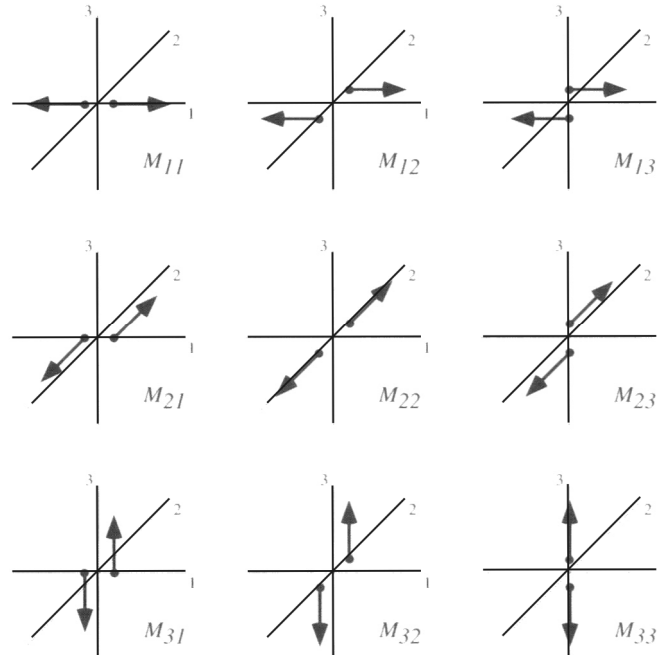


FIG. 3. Moment-tensor elements, represented as force couples (from Shearer, 1999).

FOCAL MECHANISM DIAGRAMS

A common way to represent this type of source is through classic beach-ball diagrams. These diagrams spring from the tradition in the early days of earthquake seismology to infer focal mechanism based on P -wave first-motion data (Figure 4). These diagrams present a lower-hemispheric projection of P -wave first motion data, showing the partitioning of the lower focal hemisphere into regions where the first motion is compressional (dark) from regions where the first motion is dilatational.

This presentation of earthquake focal mechanisms leads to classic beach-ball patterns that characterize different types of events such as strike-slip, normal, reverse and oblique-slip (Figure 4).

MOMENT-TENSOR INVERSION

Although first-motion analysis is still employed, most modern methods for determining focal mechanism are based on waveform inversion. As indicated by eq. (17), this approach requires very accurate knowledge of the Green's function that describes wave propagation from the source to the receiver. An exhaustive search approach may be used to determine the focal mechanism that gives the best fit (usually via least-squares) with respect to the observed data. The method generally becomes much more difficult for small events due to reduction in signal-to-noise ratio. This limitation has generally hindered the application of moment-tensor analysis to small earthquakes ($M < 4$). Since most microseismic events are in the range of $-2 < M < 2$ this represents a significant limitation for application at the reservoir scale. However, there is a tradeoff between

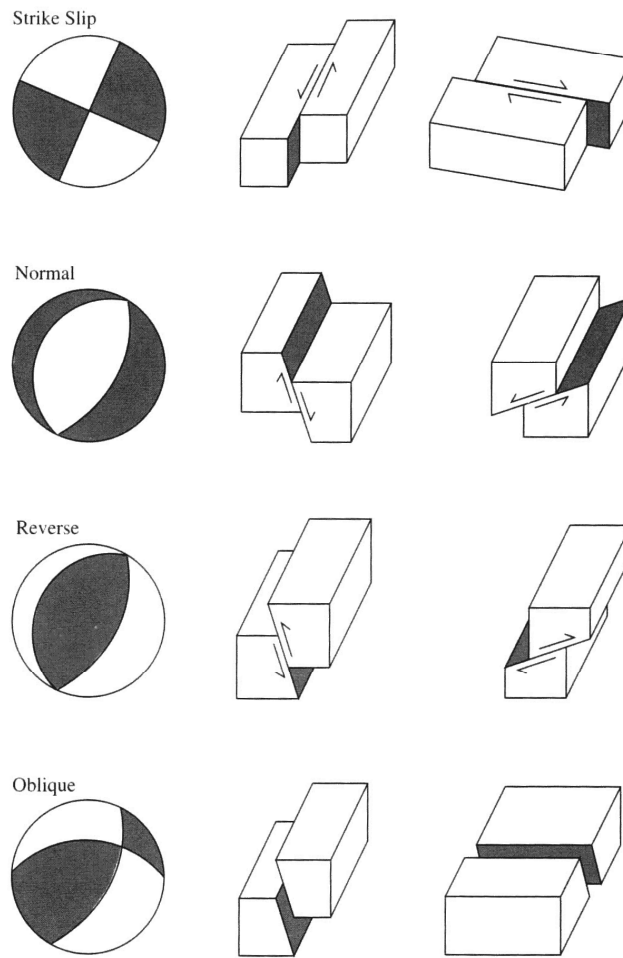
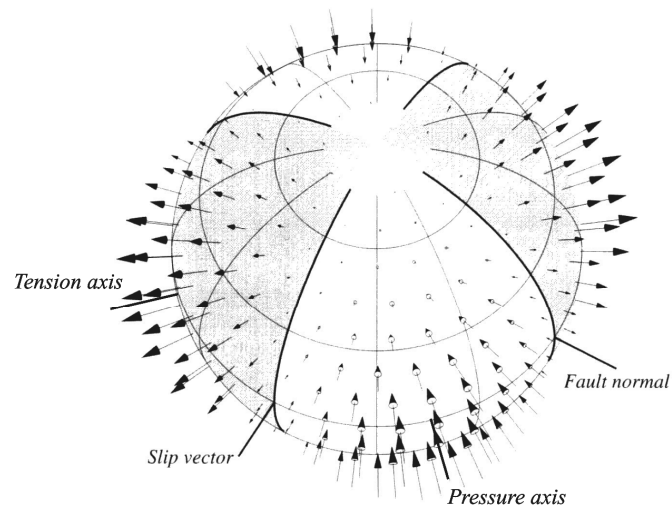


FIG. 4. P-wave radiation pattern for a double-couple event (top) and beach ball diagrams (lower-hemisphere projections) for different types of faults. From Shearer (1999).

range and magnitude, and methods have been developed that extend moment-tensor inversion to small-magnitude events (e.g., Ma and Eaton, 2008; Figure 5).

STRESS TRANSFER AND COULOMB FAILURE FUNCTION

The occurrence of any seismic event produces small, far-field deformations that perturb the ambient stress field away from the rupture site. The extent of the perturbation is dependent on the scale of rupture, and may extend to 1000's of km from a very large earthquake. This phenomenon is believed to contribute to remote triggering of earthquakes by stress transfer (Stein, 1999).

One way in which the influence of stress changes can be mapped is by calculating the so-called Coulomb failure function, given by

$$\Delta\sigma_f = \Delta\tau + \mu(\Delta\sigma_n + \Delta P), \quad (18)$$

where $\Delta\tau$ is the change in shear stress, μ is the normalized coefficient of friction in the range of [0-1], $\Delta\sigma_n$ is the change in normal stress (where the positive sign denotes tension) and ΔP is change in pore pressure. Regions of positive $\Delta\sigma_f$ are thought to be moved closer to failure after an earthquake; conversely, regions of negative $\Delta\sigma_f$ are believed to be moved farther from failure. An increase (decrease) in the Coulomb failure function may result from any combination of increased (decreased) shear stress, normal (tensional) stress, pore pressure or coefficient of friction.

The Coulomb failure function can be computed based on modeled far-field strains from an earthquake (Stein, 1999). For examples, Fig. 6 shows the Coulomb failure function computed for the 1994 $M_w = 6.7$ Northridge earthquake in California. Although stress changes are small (on the order of 1 bar), earthquake aftershocks are observed to cluster within regions of positive $\Delta\sigma_f$. More importantly, the rates of seismicity have been shown to correlate with changes of $\Delta\sigma_f$ in a statistically significant manner (Stein, 1999).

Microseismic events, including those associated with hydraulic fracturing and fluid injection, will produce far-field stress perturbations on a much smaller scale. Future research will investigate whether the Coulomb failure function provides a useful diagnostic measure of stress transfer associated with induced seismicity from hydraulic fracturing and fluid injection.

CONCLUSIONS AND FUTURE WORK

This tutorial briefly reviews a number of ways in which natural source mechanisms can be characterized. The methods covered in this review include various magnitude scales, seismic moment and moment tensors.

These methods form the basis for planned future microseismic investigations at the reservoir scale. Given sufficiently high SNR and well defined instrument response, it should be possible to apply spectral methods used in earthquake seismology to derive

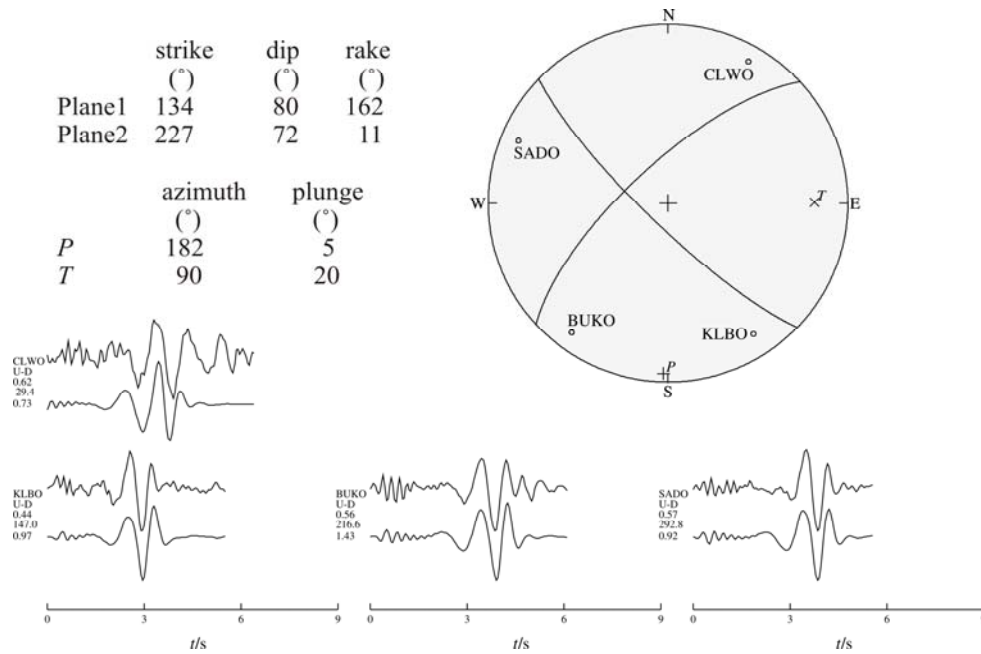


FIG. 5. Example of moment-tensor inversion for a small ($M \sim 2$) event, showing focal mechanism and comparison of observed and modeled waveforms. The highest-amplitude arrival is a Rayleigh wave. From Ma and Eaton (2008).

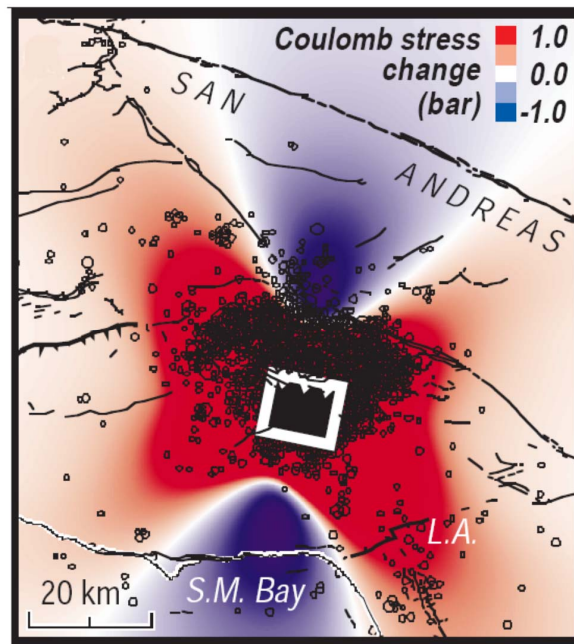


FIG. 6. Coulomb failure function and aftershocks for the 1994 Northridge earthquake (Stein, 1999). Aftershocks tend to concentrate in areas of positive $\Delta\sigma_f$.

important inferences, including approximate source radius and stress drop. Moreover, moment-tensor inversion methods adapted to low-magnitude events (Ma and Eaton, 2007) may provide a way to discriminate between slip on a fracture surface and

generation of new tensile fractures. Finally, the analysis of stress transfer using the Coulomb failure function may provide insights that are useful for understanding far-field induced seismicity in scenarios of practical interest.

REFERENCES

- Beresnev, I., 2001, What we can and cannot learn about earthquake sources from the spectra of seismic waves: *Bulletin of the Seismological Society of America*, **91**, 397–400.
- Brune, J. N., 1970, Tectonic stress and the spectra of seismic shear waves from earthquakes: *Journal of Geophysical Research*, **75**, 4997–5009.
- Brune, J. N., 1971, Correction: *Journal of Geophysical Research*, **76**, 5002.
- Bullen, K.E., and Bolt, B.A., 1985, *An Introduction to the Theory of Seismology*: Cambridge University Press.
- Lay, T., and Wallace, T.C., 1995, *Modern global seismology*: Academic Press.
- Ma, S., and Eaton, D.W., 2007, Western Quebec seismic zone (Canada): Clustered, mid-crustal seismicity along a Mesozoic hotspot track: *Journal of Geophysical Research*, **112**, B06305, doi: 10.1029/2006JB004827.
- Ma., S., and Eaton, D.W., 2008, Anatomy of a small earthquake swarm in southern Ontario, Canada: *Seismological Research Letters*, in press.
- McGillivray, P., 2005, Microseismic and time-lapse seismic monitoring of a heavy oil extraction process at Peace River, Canada: *CSEG Recorder*, **30**, No. 1, 5-9.
- Nolen-Hoeksema, R.C., and Ruff, L.J., 2001, Moment tensor inversion of microseisms from the B-sand propped hydrofracture, M-site, Colorado: *Tectonophysics*, **336**, 163-181.
- Nuttli, O.W., 1973, Seismic wave attenuation and magnitude relations for eastern North America: *Journal of Geophysical Research*, **78**, 876-885.
- Rutledge, J.T., and Phillips, W.S., 2003, Hydraulic stimulation of natural fractures as revealed by induced microearthquakes, Carthage Cotton Valley gas field, east Texas: *Geophysics*, **68**, 441-452.
- Sasaki, S., and Kaieda, H., 2002, Determination of stress state from focal mechanisms of microseismic events induced during hydraulic injection at the Hijiori hot dry rock site: *Pure and Applied Geophysics*, **159**, 489-516.
- Shearer, P.M., 1999. *Introduction to Seismology*: Cambridge University Press.
- Stein, R.S., 1999, The role of stress transfer in earthquake occurrence: *Nature*, **402**, 605-609.
- Velasco, A.A., Ammon, C., and Lay, T., 1994, Empirical green function deconvolution of broadband surface waves: Rupture directivity of the 1992 Landers, California ($M_w = 7.3$), earthquake: *Bulletin of the Seismological Society of America*, **84**, 735-750.
- White, D.J., Burrowes, G., Davis, T., Hajnal, Z., Hirsche, K., Hutcheon, I., Majer, E., Rostron, B., and Whittaker, S., 2004, Greenhouse gas sequestration in abandoned oil reservoirs: the IEA Weyburn pilot project: *GSA Today*, **14**, No. 7, 4-10.